Yerbilimleri, 31 (1), 33–43
Hacettepe Üniversitesi Yerbilimleri Uygulama ve Araştırma Merkezi Dergisi
Journal of the Earth Sciences Application and Research Centre of Hacettepe University

An experimental and theoretical study of the piping failure of slope failure dams

Heyelan barajlarının sızma yenilmesi üzerine deneysel ve kuramsal bir çalışma

Ömer AYDAN

Tokai University, Department of Marine Civil Engineering, Shizuoka, JAPAN

Geliş *(received)* : 01 Aralık *(December)* 2009
Kabul *(accepted)* : 26 Ocak *(January)* 2010

ABSTRACT

The failure of slopes along rivers often results in dams of debris material. If such dams with a significant volume fail, they may cause secondary disasters downstream. The author has been involved with this problem since his reconnaissance visits to the damaged areas of Kashmir after the 2005 Azad Kashmir earthquake. This earthquake caused one of the largest dams of slope failure, which occurred near Hattian. This study reports the theoretical and physical experiments on the piping failure of such deposits that were carried out. These studies are described in this article and theoretical estimations are compared with experimental results. The comparisons imply that the experimental results generally confirm the theoretical estimations. However, there is a difference between the hydraulic gradients for initiation and for total failure due to piping, which may be attributable to the difference between the actual fluid velocity and the averaged velocity used in D'Arcy's law.

Keywords: Earthquake, experiment, piping failure, slope failure dam, theory.

ÖZ

Şev yenilmeleri çoğu kez heyelan setlerinin (barajlarının) oluşumuna neden olur. Heyelan barajlarının oldukça büyük olması halinde, bunlar barajın alt bölgelerinde ikincil doğal afetlere neden olabilirler. Yazar, 2005 Hür Kaşmir depreminin hasar incelemeleri sonrasında bu konuyla ilgilenmeye başlamıştır. Kaşmir depreminde yüksekliği 160 m'ye ulaşan heyelan barajı Hattian yakınlarında oluşmuştur. Yazar, bu konu ile ilgili olarak laboratuvarda değişik kum örnekleri ile Kaşmir depreminde Muzaffarabad yakınlarında meydana gelen büyük bir heyelandan aldığı malzeme örneklerini kullanarak fiziksel model deneyleri yapmıştır. Bunun yanı sıra, konunun kuramsal kısmı da incelenmiştir. Bu makalede, deneysel çalışma sonuçları sunulmuş ve kuramsal yaklaşım sonuçları ile karşılaştırılmıştır. Kuramsal sonuçlarla deneysel sonuçların birbirleriyle uyumlu olduğu görülmekle birlikte, sızma yenilmesinin başlangıcı ile tümden yenilme için hidrolik eğimin farklı olduğu gözlenmiştir. Bu farklılık, büyük bir olasılıkla, gerçek akışkan hızı ile D'Arcy yasasındaki ortalama akışkan hızları arasındaki farklılıkla ilişkilendirilebilir.

Anahtar Kelimeler: *Deprem, deney, sızma yenilmesi, heyelan barajları, kuram.*

Ö. Aydan
E-mail: aydan@scc.u-tokai.ac.jp

INTRODUCTION

Large slope failures along rivers often result in dams of debris material (Figure1). The piping failure of soil deposits is of great concern with regard to the stability of earth and rockfill dams, embankments and natural slope failure dams. Such failures may generally lead to catastrophic damage to downstream settlements and environments. Historically, the most spectacular example of piping failure is the failure of the Teton dam in the USA. In addition, there are many examples of piping and overtopping failure of landslide or glacier lakes in mountainous areas such as the Himalayas, Andes and Rockies (see Singh (1996) for details) (Figures 1 and 2).

The M_s=8 Wenchuan earthquake in 2008 caused the formation of 34 quake lakes. Among these 34 quake-lakes, three that formed in Anxian, Qingchuan and Beichuan counties were of great scale and were caused mainly by the planar sliding failure of mountains (i.e. Aydan et al., 2009a). The biggest quake-lake of all was the Tangjiashan "quake lake", which was formed by the collapse of a section of Tangjiashan Mountain. Tangjiashan quake-lake was formed 2 km from Beichuan and at its peak was 803 m long by 612 m wide and 70-124 m high. The estimated volume of water of the Tangjiashan quake-lake was 250 Mm^3. Luckily, nobody was killed by the collapse of the slope failure dam.

Historically, a large slope failure occurred in the Kangding-Luding area of Sichuan, China in 1786. This large slope failure, caused by an M=7.75 earthquake, created a large slope failure dam on the Dadu River (Dai et al., 2004), and the sudden failure of this slope failure dam resulted in catastrophic downstream flooding ten days after the earthquake. It was reported that more than 100,000 people lost their lives. This may be the most disastrous event ever caused by failure of a slope failure dam. The slope failure dam was about 70 m high, and it created a lake with a water volume of about 50×10^6 m^3 and an area of about 1.7 km^2. The dam failed suddenly due to a major aftershock on June 10, 1786.

The highest slope failure dam is the Usoi slope failure dam, named after the village of Usoi, which was completely buried by the 1911 large slope failure in Tajikistan. It has a total volume estimated at approximately 2 km^3 with a maximum height above the original valley floor of 500 m to 700 m (i.e. Risley et al., 2006). The lake that formed behind the Usoi dam rose at an initial rate of approximately 75 m/y. This lake was named after the village of Sarez, that was drowned by the rising water. Lake Sarez is now over 60 km in length with a maximum depth in excess of 500 m and a total volume of approximately 17 km^3. The Usoi dam is the highest natural dam on earth. The level and the stability of this dam have been continuously monitored.

There are also many slope failure dams in Turkey. The recent Kuzulu slope failure also caused a small lake (see Figure 1), which was later breached (Ulusay et al., 2007). The gigantic planar rock slope failure blocked the Tortum River and formed the largest landslide-dammed lake in Turkey, measuring 8500 m in length, 2500 m in width and having a surfacial area of 6.77 km^2 (i.e. Duman, 2009). The slope failure occurred as a rapid planar sliding failure in the Cretaceous interbedded limestones with clastics. The surface of the sliding formed along the bedding plane. The dam was estimated to have a maximum height of 270m and impounded 1820km^2 of mountainous drainage area, forming a lake with 538million m^3 of water on the Tortum River. Duman (2009) claimed that the landslide could be more than 300 years old. Luckily, the dam created by this landslide has not failed for at least 3 centuries.

In July 2003 a landslide occurred on the Pareechu stream of the Satluj River in Tibet (see Figure 2). The slope failure blocked the river for about 400 m and formed a lake that eventually breached. The lake was 2,100 m long, 1,100 m wide and about 40 m deep. NASA (2005) captured the formation, growth and collapse process of the Pareechu slope failure dam from 2003 till 2005, as seen in Figure 2. Although nobody was killed, by virtue of remote and in-situ monitoring of the growth of the dam lake, the breached slope failure dam caused some damage in Tibet and India (Gupta and Shah, 2008).

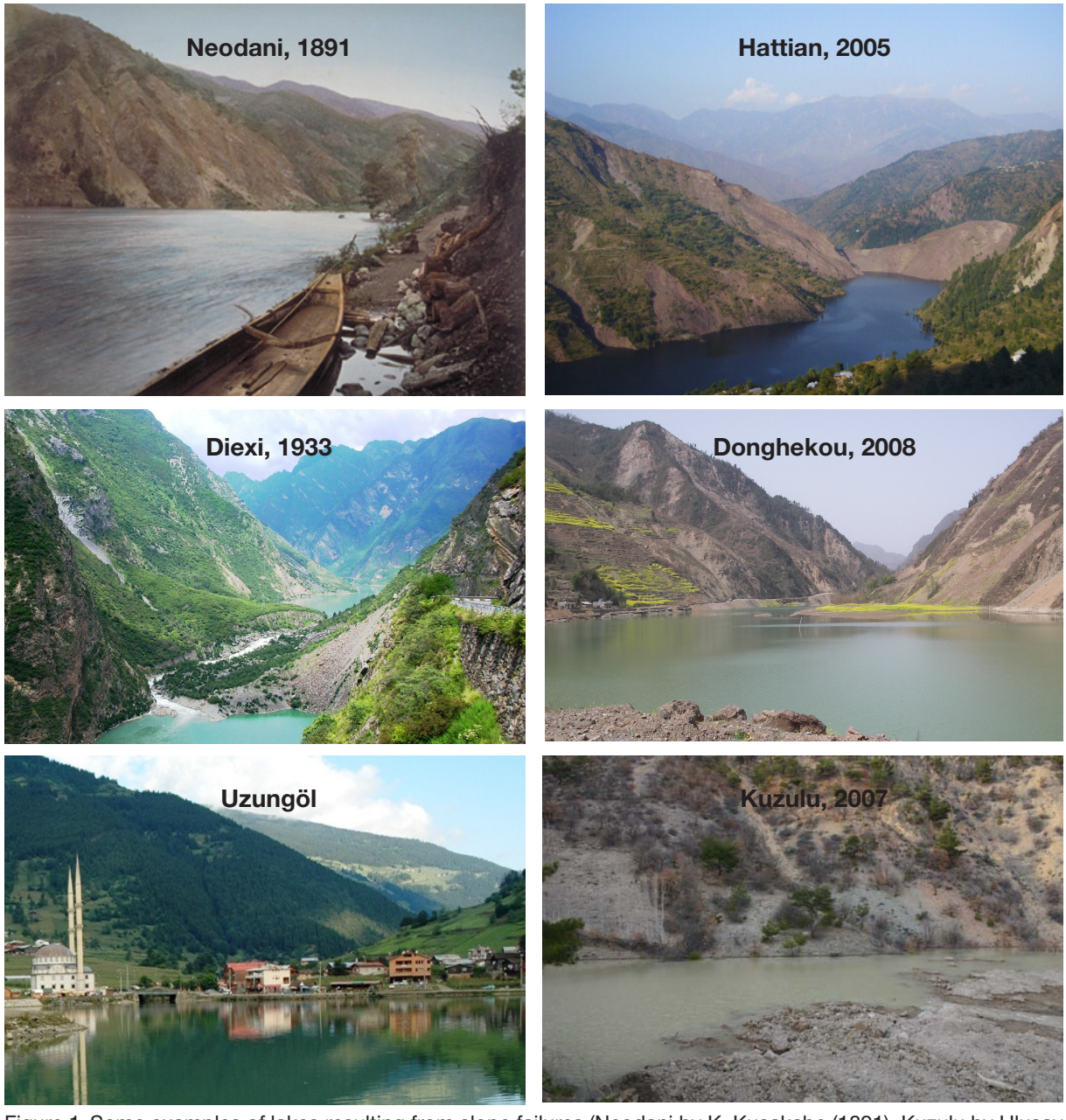

Figure 1. Some examples of lakes resulting from slope failures (Neodani by K. Kusakabe (1891), Kuzulu by Ulusay et al. (2007) and other photographs by the author. Dates in the picture correspond to the event dates).
Şekil 1. Heyelan sonucu oluşmuş gölcüklere örnekler (Fotoğraflar: Neodani (K. Kusabe, 1891), Kuzulu (Ulusay vd., 2007) diğerleri (yazar). Resimlerdeki tarihler oluş tarihini gösterir).

The author recently investigated the areas affected by the 2005 Kashmir earthquake and the 2008 Wenchuan earthquake (Aydan et al., 2009a, b). These earthquakes caused many rock slopes, some which resulted in landslide dams. Some of these landslide dams are already breached while the one in Hattian still poses a huge catastrophic risk to the downstream area. The author got interested in this phenomenon and carried out some experimental and theoretical studies. This article describes the outcomes of these studies.

EXPERIMENTS

Two different experimental set-ups were used in order to understand the conditions governing the piping phenomenon. The details of the cha-

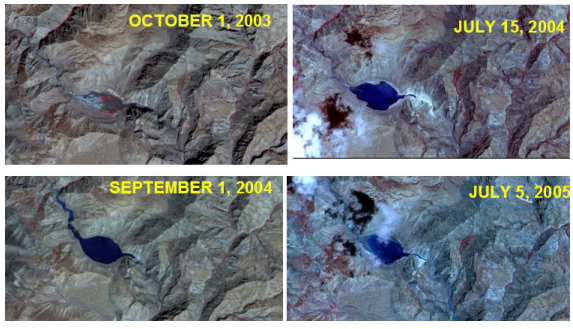

Figure 2. Growth and failure of the slope failure dam of Pareechu (Tibet) (arranged from images taken by NASA at different times).

Şekil 2. Pareechu heyelan barajının büyümesi ve yıkılması (NASA tarafından farklı zamanlarda elde edilmiş görüntülerden derlenmiştir).

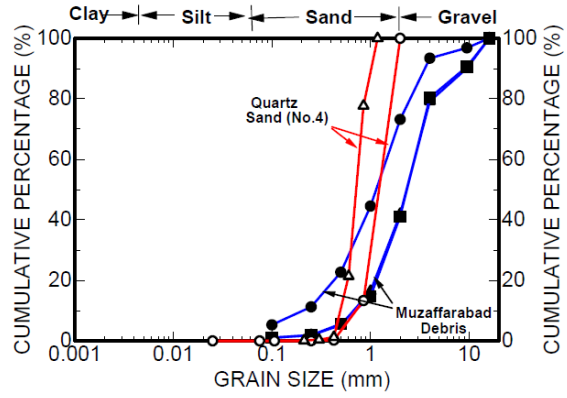

Figure 3. Grain size distribution of experimental materials.

Şekil 3. Deneylerde kullanılan malzemenin tane boyu dağılımı.

racteristics of materials, experimental set-ups, and experimental results are given below.

Characteristics Materials

Two different materials used in the experiments were commercially available quartz sand (No.4) and slope failure debris from Muzaffarabad in Kashmir. Slope failure debris material was crushed dolomite and constituted the fault zone (Aydan et al., 2009b). Grain size distributions and properties of experimental materials are shown in Figure 3 and given in Table 1, respectively. The hydraulic conductivity of the debris material is very similar to the permeability of the sand in view of the grain size distribution of the materials.

Experimental Set-ups

Co-centric cylindrical set-up

A co-centric cylindrical set-up was used to study the conditions of the piping phenomenon (Figure 4). The diameters of the outer and inner acrylic cylinders were 120 mm and 75 mm, respectively. The soil column height was 80 mm and the inner cylinder was embedded to a depth of 35 mm from the soil surface. Two pressure sensors were used to measure the water pressure near the surface of the soil in the inner and outer cylinders. With this set-up, it was possible to measure the head difference, since it is impossible to prevent seepage during the water head rise. Water was pumped into the inner cylinder through a hose using an electrical pump from a reservoir. A 30 mm thick sponge layer was placed on the top of the soil column of the inner cylinder, in order to prevent erosion by the pumped-in water and to attain uniform water pressure head increase. In addition, an Acoustic Emission (AE) sensor was attached to the outer surface of the outer cylinder in order to assess the time of piping failure.

Slope failure dam experiments

Slope failure dam piping failure experiments were carried out by using a 100 m wide, 200 m high and 300 m long acrylic tank. The tank had a 105 mm wide reservoir and a 30 mm thick sponge wall, which provided a uniform seepage into the soil and prevented erosion during water head rise, dividing the tank into two compartments. The height of the earth dam was about 100-110 mm with a slope inclination of 39-43° and a crest width of 30-40 mm. Two pressure sensors were used to measure the water pressure near the dam toe and in the water reservoir (Figure 5). Similar to the previous set-up, it was possible to measure the head difference since it is very difficult to prevent seepage during the water head rise. The water was pumped into the reservoir through a hose using an electrical pump from a reservoir. In addition, an AE sensor was attached to the outer surface of the tank in order to assess the time of piping failure.

Table 1. Properties of samples used in experiments.
Çizelge 1. Deneylerde kullanılan malzemelerin özellikleri.

Material	Dry unit weight (kN/m^3)	Void ratio (%)	Porosity (%)	Mean grain size D_{50} (mm)	Friction angle (°)	Hydraulic conductivity (cm/s)
Sand	14.6	78.09	43.85	0.69-1.27	32-35	1.3-1.5x10^{-1}
Debris	14.6	56.44	36.07	1.15-2.30	35-39	1.76x10^{-1}

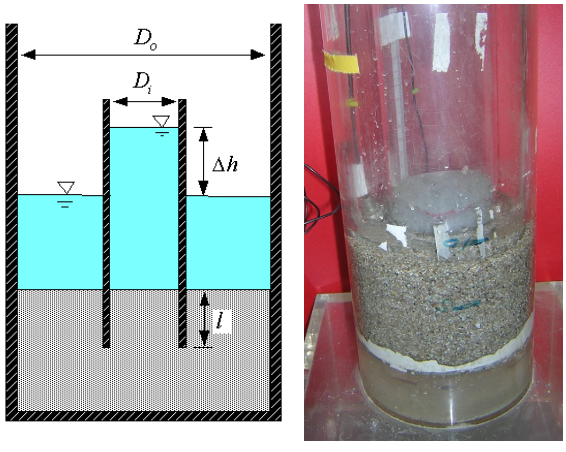

Figure 4. Co-centric cylindrical experimental set-up.
Şekil 4. Eş merkezli silindirik deney düzeneği.

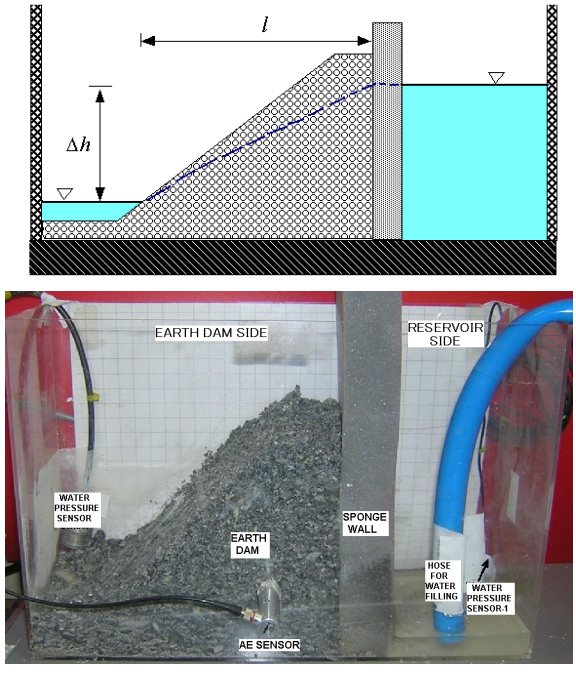

Figure 5. (a) Cross section of the model, and (b) slope failure dam experimental set-up.
Şekil 5. (a) Modelin kesiti ve (b) heyelan barajı deney düzeneği.

Experiments and Results

Co-centric cylinder tests

Co-centric cylinder tests were performed on commercially available quartz sand soil (No.4). Figures 6 and 7 show various stages of an experiment and some of measured responses during experiments, respectively. The depth of the embedment of the inner cylinder into soil, the water head differences and the hydraulic gradients at the initiation and failure of piping are summarized in Table 2. As seen in Figure 6, the initial phase of the seepage was almost uniform. When the piping phenomenon started to take place near the outer perimeter of the cylinder a large flow started to occur. This large water flow enlarged erosion and eventually resulted in a large plume of the mixture of sand and water.

Figure 7 shows the water rise of the upper reservoir, head difference and AE responses of the three model tests. The increase in head difference becomes particularly non-linear at a critical level, which corresponds to the piping initiation. The water head difference decreases monotonically following the failure of the slope failure dam. Large gradient changes of the cumulative AE response occur at the initiation and at the failure of the piping phenomenon. Table 2 summarizes the geometrical parameters and hydraulic gradients at the initiation and failure of the piping phenomenon for the co-centric cylindrical experiments. The ratio of the hydraulic gradient at initiation to that at the failure of the piping phenomenon ranges between 78% and 94% for the model tests.

Slope failure dam piping failure experiments

In these experiments, two soil samples were used. One sample was the same as that used in the previous tests and it comprised quartz sand commercially available soil (No.4). The se-

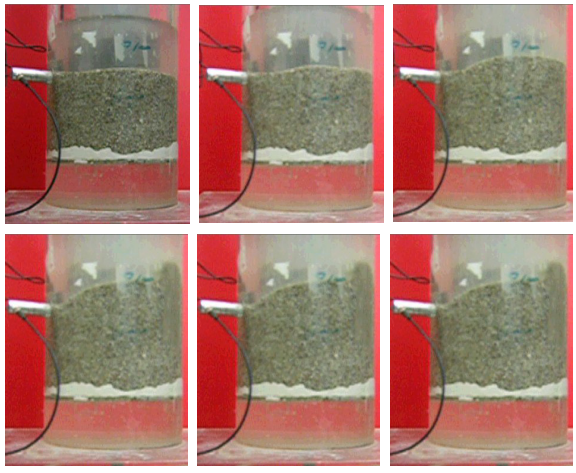

Figure 6. Views of piping failure at different times during an experiment.
Şekil 6. Deney sırasında sızma yenilmesinin değişik zamanlardaki görüntüleri.

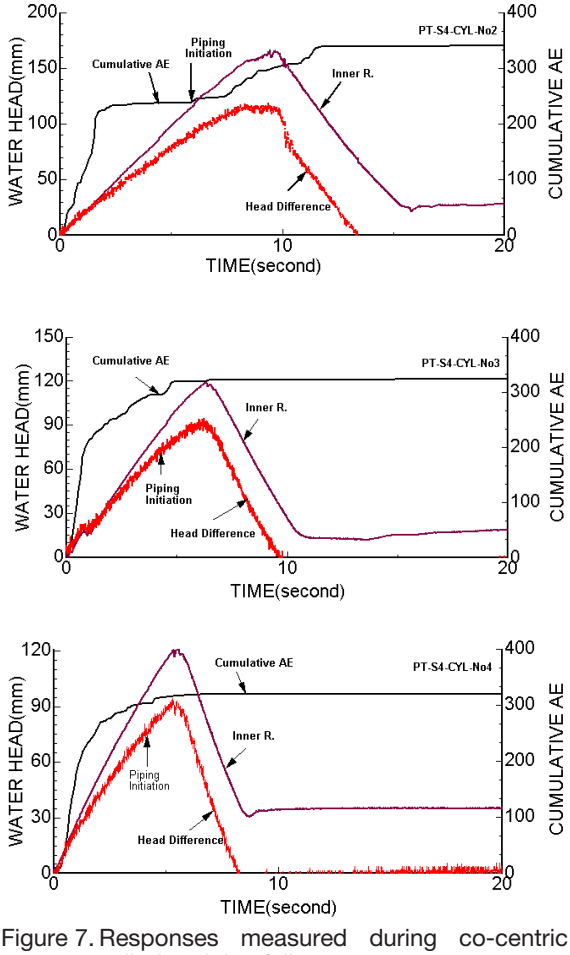

Figure 7. Responses measured during co-centric cylinder piping failure tests.
Şekil 7. Eş-merkezli silindirik sızma yenilmesi deneylerinde ölçülen davranışlar.

cond soil sample was from Muzaffarabad where dolomitic limestone slope failed during the earthquake and blocked the Neelum Valley for a short time, it being breached later on. Figure 8 shows various stages of a piping experiment on the Muzaffarabad debris dam model. Figures 9 and 10 show some of the measured responses during the experiments. Tables 3 and 4 summarize the experimental results on dam models consisting of sand No.4 and Muzaffarabad debris material.

As seen in Figure 8, the initial phase of the seepage is almost uniform. When the piping phenomenon starts to take place, a large water flow starts to occur at mid height of the slope failure dam. This large water flow enlarges erosion and eventually results in the failure of the slope failure dam.

Figures 9 and 10 show the water rise of the upper reservoir, head difference and AE responses on the model tests with the use of No.4 sand and Muzaffarabad debris. Particularly notable is the fact that the increase in head difference tends to be non-linear at a critical level, which is indicated as the piping initiation. While the water head difference decreases monotonically for the model tests using No.4 sand, there is a sudden decrease in water head difference when the failure of the slope failure dam occurs.

Tables 3 and 4 summarize the geometrical parameters and hydraulic gradients at the initiation and at the failure of the piping phenomenon. The ratio of the hydraulic gradient at initiation to that at failure ranges between 85% and 93% for the model tests using No.4 sand. On the other hand, the ratio of the hydraulic gradient at initiation to that at failure ranges between 54% and 79% for the model tests using the Muzaffarabad debris. This difference may be attributable to a difference in the non-uniform distribution of the permeability characteristics of the model materials.

THEORETICAL BACKGROUND TO THE PIPING FAILURE PHENOMENON

Theoretical Fundamentals

The piping failure phenomenon is as a result of the dislocation of particles from the slope failu-

Table 2. A summary of conditions of co-centric cylindrical experiments and measured results.
Çizelge 2. Eş merkezli silindrik model deney koşulları ve ölçülen sonuçlara ilişkin özet bilgi.

Test No.	Embedment (*l*) (mm)	Water head difference at initiation (mm)	Water head difference at failure (mm)	Hydraulic gradient at	
				Initiation	Failure
PT_S4_CYL_No1	35	88.9	94.7	2.54	2.71
PT_S4_CYL_No2	35	90.2	115.2	2.58	3.29
PT_S4_CYL_No3	30	73.0	90.7	2.43	3.02
PT_S4_CYL_No4	31	75.6	91.6	2.44	2.95

Table 3. A summary of conditions of slope failure dam experiments for No.4 sand and measured results.
Çizelge 3. 4 no.lu kum heyelan barajı deney koşulları ve ölçülen sonuçlara ilişkin özet bilgi.

Test No.	Base length (l) (mm)	Water head difference at initiation (mm)	Water head difference at failure (mm)	Hydraulic gradient at	
				Initiation	Failure
PT_S4_DAM_No1	123	78.7	84.80	0.64	0.69
PT_S4_DAM_No2	123	80.8	88.2	0.66	0.72
PT_S4_DAM_No3	123	77.7	88.6	0.63	0.72

Table 4. A summary of experimental conditions for Muzaffarabad slope failure dam debris material and measured results.
Çizelge 4. Muzaffarabad heyelan molozu için deneysel koşullar ve ölçülen sonuçlara ilişkin özet bilgi.

Test No.	Base length (l) (mm)	Water head difference at initiation (mm)	Water head difference at failure (mm)	Hydraulic gradient at	
				Initiation	Failure
PT_MD_DAM_No1	120	66.5	84.1	0.55	0.70
PT_MD_DAM_No2	120	58.6	81.5	0.49	0.68
PT_MD_DAM_No3	120	39.6	72.7	0.33	0.61

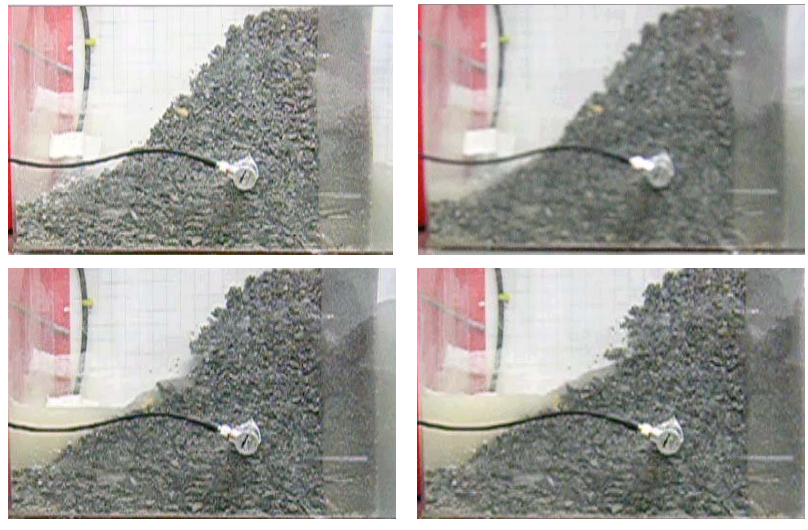

Figure 8. Various stages of the earth dam piping model test on Muzaffarabad slope debris material.
Şekil 8. Muzaffarabad moloz malzemesi üzerinde yapılan baraj sızma yenilme deneyi görüntüleri.

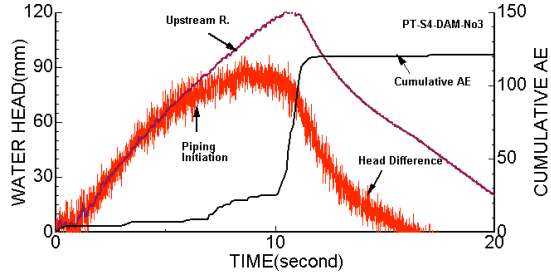

Figure 9. Responses measured during an experiment on a dam model using sand No.4.
Şekil 9. 4 no.lu kum kullanılarak yapılan baraj modeli deneylerinde ölçülen davranışlar.

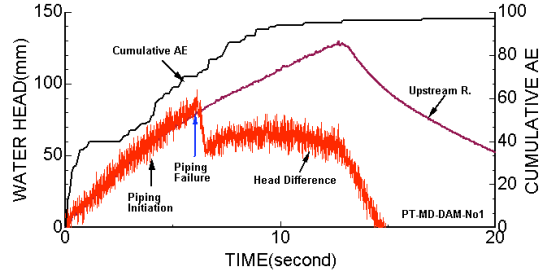

Figure 10. Responses measured during an experiment on a dam model using Muzaffarabad debris material.
Şekil 10. Muzaffarabad moloz malzemesi kullanılarak yapılan baraj modeli deneylerinde ölçülen davranışlar.

re dam under the action of seepage forces. The drag stress (seepage stress) on a per unit soil mass under a seepage field gradient is given in the following form (i.e. Biot, 1941, 1962).

$$\xi_{sf} = -\frac{\eta}{k}\bar{\mathbf{v}}_r \tag{1}$$

Where; k, η and $\bar{v}_r$ are permeability (areal), viscosity and average relative velocity of fluid with respect to solid skeleton. The average relative velocity of fluid is generally expressed through D'Arcy's law as follows:

$$\bar{\mathbf{v}}_r = -\frac{k}{\eta} \cdot \mathbf{p} \tag{2}$$

where **p** is fluid pressure. Inserting Equation (2) into (1) yields the following relation.

$$\xi_{sf} = -\nabla \cdot \mathbf{p} \tag{3}$$

In one dimensional form, one may write the following

$$\xi_{sf} = -\frac{\partial p}{\partial x} \tag{4}$$

Let us assume that pressure is given in terms of fluid density (ρ) and fluid head (h) as follows:

$$p = pgh \tag{5}$$

where, g is gravitational acceleration. With the use of Equation 5, Equation (4) becomes

$$\xi_{sf} = -\rho g \frac{\partial h}{\partial x} \tag{6a}$$

If the fluid is water, this equation may be written in terms of unit weight of water as follows.

$$\xi_{sf} = -\gamma_w \frac{\partial h}{\partial x} \tag{6b}$$

Equation 6 is the relation which appears commonly in many soil mechanics textbooks.

Formulation of the Co-centric Cylindrical Piping Experiment

Let us consider two co-centric cylinders which are used for piping failure tests (see Figure 4). Furthermore, let us assume that the water head is increased during experiments. The force exerted at the base of the inner cylinder causes the movement of the soil column in the inner and outer cylinders. Under this circumstance, one may write the following relation:

$$\gamma_w \Delta h A_i - \gamma_{sub} \Delta x A_o = 0 \tag{7}$$

where $\gamma_{sub} = \gamma_{sat} - \gamma_w$ and $\Delta x = l$

Since γ_{sat} is equivalent to $\gamma_{sat} = (1-n)\gamma_g + n\gamma_w$, γ_{sub} may be given in the following form

$$\gamma_{sub} = (1-n)(\gamma_g - \gamma_w) \text{ or } \gamma_{sub} = \frac{(G_s - 1)}{1+e}\gamma_w \quad (8)$$

where, γ_g is unit weight of solid grains. Porosity (*n*) and void ratio (*e*) are related to each other in the following form

$$n = \frac{e}{1+e} \quad (9)$$

Thus, the following identity holds from Equations 7 and 8 at the time of piping failure.

$$\frac{\Delta h}{\Delta x} = \frac{G_s - 1}{1+e}\frac{A_o}{A_i}\gamma_w \quad (10)$$

Formulation of the Dam Piping Experiment

Next, a special form of the slope failure earth dam was considered, as illustrated in Figure 5. The force equilibrium per unit width for this particular case may be written as:

$$\frac{\gamma_w \Delta h^2}{2} - \frac{\gamma_{sub}\Delta h l}{2} = 0 \quad (11)$$

where h and l are water head and base length. With the use of Equations 8 and 11, one can easily obtain the following relation for the piping failure.

$$\frac{\Delta h}{l} = \frac{G_s - 1}{1+e}\gamma_w \quad (12)$$

Equation 12 is well-known as the critical hydraulic gradient of Terzaghi (1929, 1943). As noted from the relations above, the size distribution and permeability of the dam material do not play any role in the resistance against piping failure. Another alternative formulation may be based on the utilization of Stoke's law. The drag force acting on a particle with an average diameter D can then be given in the following form:

$$dF = 3\pi D\eta v_r \quad (13)$$

where η is fluid viscosity. The effective weight of a spherical particle can be written as follows:

$$dW' = (1-n)(\gamma_s - \gamma_w)\frac{\pi D^3}{6} \quad (14)$$

Equating Equations 13 and 14 together with the use of Equations 2 and 5, one can easily obtain the following relation:

$$\frac{\Delta h}{l} = \frac{G_s - 1}{1+e}\gamma_w \frac{D^2}{18k} \quad (15)$$

The permeability coefficient k may be related to mean grain size *D* (i.e. Kozeny-Karman relation, Aydan et al., 1997), as follows:

$$k = \frac{1}{A}D^2 \quad (16)$$

Inserting Equation 16 into Equation 15 yields the following expression:

$$\frac{\Delta h}{l} = \frac{G_s - 1}{1+e}\gamma_w \frac{A}{18} \quad (17)$$

There are many suggestions for the value of *A*. The appropriate one should be used taking the ground conditions into consideration. However, the value of *A* generally ranges between 12 and 20.

COMPARISONS AND DISCUSSIONS

Figure 11 compares the computational results with the experimental results for the co-centric cylindrical set-up. Theoretical predictions were based on Equation 10 with the use ground material with the properties given in Table 1. The experimental values for the initiation and failure of the piping phenomenon are higher than those of the theoretical estimations. Furthermore, there is a slight scattering. The difference may be attributed to the frictional resistance between soil and cylinder walls as well as to the dif-

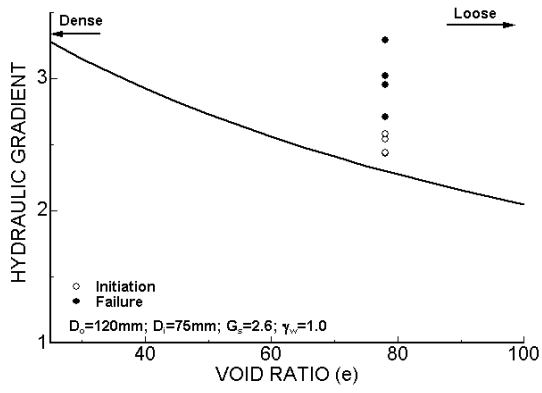

Figure 11. Comparison of co-centric cylindrical model experimental results with theoretical estimations.

Şekil 11. Eş merkezli silindirik model deneysel sonuçlarının kuramsal sonuçlarla karşılaştırılması.

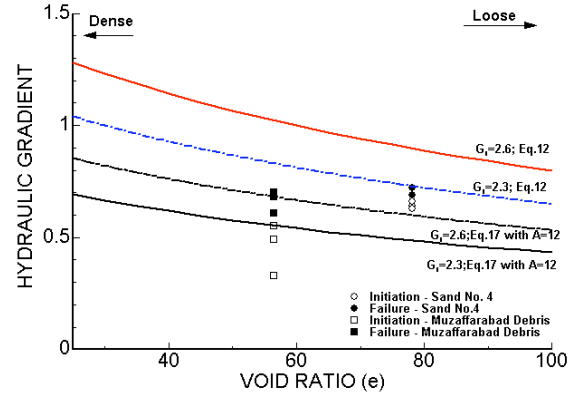

Figure 12. Comparison of slope failure dam model experimental results with theoretical estimations.

Şekil 12. Heyelan barajları model deneysel sonuçlarının kuramsal sonuçlarla karşılaştırılması.

ference between the actual and averaged velocities of fluid.

Figure 12 compares the computational results with experimental results for the co-centric cylindrical set-up. Equations 12 and 17 were used for theoretical estimations with the use of ground materials with the properties given in Table 1. The experimental values for the initiation and failure of the piping phenomenon are lower than those of the theoretical estimations. The specific weight of material varied between 2.3 and 2.6, as the specific weight of the Muzaffarabad debris is about 2.3. The estimations based on Equation 12 are considerably higher than the experimental values. However, Equation 17 yields better estimations for experimental results. Furthermore, there is a slight scattering. The scattering may be attributed to the slight differences in ground material in each experiment.

CONCLUSIONS

Piping failure of earth or rock fill dams, as well as slope failure dams, is quite important for the safety of settlements downstream as well as for the protection of property. Although dams are constructed with great attention to this problem, slope failure dams are a result of natural disasters and the resulting mass is very complex in geometrical distribution of particles as well as in seepage properties. This problem has been well known for a long time. Nevertheless, it is still difficult to assess the overall stability of slope failure dams due to their complex geometry and the distribution of their particles. Experiments on commercial sand as well as on natural slope failure debris indicated that theoretical relations may be applied to predict piping failure conditions. Nevertheless, there is a difference between the hydraulic gradients for initiation and total failure due to piping. The initiation of piping failure starts at lower hydraulic gradients. This may be attributable to a difference between the actual fluid velocity and the averaged velocity used in D'Arcy's law.

When, upon complete inundation, slope failure dams are stable, the breach of such dams may occur by overtopping. This is a more complex phenomenon on which some experimental and theoretical studies have been undertaken. Nevertheless, further studies of this problem are necessary. The well-publicized breach of the Tangjiashan slope failure dam, which was caused by the 2008 Wenchuan earthquake, showed the importance of this problem.

REFERENCES

Aydan, Ö., Üçpırtı, H., and Ulusay, R., 1997. Theoretical formulation of Darcy's law for fluid flow through porous and/or jo-

inted rock and its validity. Kaya Mekaniği Bülteni, 13, 1-18 (in Turkish).

Aydan, Ö., Hamada, M., Itoh, J., and Ohkubo, K., 2009a. Damage to civil engineering structures with an emphasis on rock slope failures and tunnel damage induced by the 2008 Wenchuan earthquake. Journal of Disaster Research, 4 (2), 153-164.

Aydan, Ö., Ohta, Y., and Hamada, M., 2009b. Geotechnical evaluation of slope and ground failures during the 8 October 2005 Muzaffarabad earthquake in Pakistan. Journal of Seismology, 13 (3), 399-413.

Biot, M.A., 1941. General theory of three-dimensional consolidation. Journal of Applied Physics, 12, 155-164.

Biot M.A., 1962. Mechanics of deformation and acoustic propagation in porous media. Journal of Applied Physics, 33 (4), 1482.1498.

Dai, F.C., Lee, C.F., Dengand, J.H., and Tham, L.G.., 2005. The 1786 earthquake-triggered landslide dam and subsequent dam-break flood on the Dadu River, southwestern China. Geomorphology, 65 (3-4), 205-221.

Duman, T.Y., 2009. The largest landslide dam in Turkey: Tortum landslide. Engineering Geology, 104 (1-2), 66-79

Gupta, V., and Sah, M.P., 2008. Impact of the Trans-Himalayan landslide lake outburst flood (LLOF) in the Satluj catchment, Himachal Pradesh, India. Natural Hazards, 45, 379-390.

Kusakabe, K., 1891. Neoya quake-lake. In the album of Japanese old photographs in Bakumatsu - Meiji period, Nagasaki University Library Collection.

NASA, 2005. Landslide lake in Tibet Floods India. ASTER images taken in 2003, 2004 and 2005 by LANDSAT 7. http://earthobservatory.nasa.gov/NaturalHazards/

Risley, J., Walder, J., and Denlinger, R., 2006. Usoi Dam wave overtopping and flood routing in the Bartang and Panj Rivers, Tajikistan. USGS, Water-Resources Investigations Report 03-4004.

Singh, V.P., 1996. Dam Breach Modeling Technology. Kluwer, Dordrecht.

Terzaghi, K., 1929. Effect of minor geologic details on the safety of dams. Bulletin of American Institute of Mining and Metallurgical Engineers, Technical Publication 215, Class I, Mining Geology, 26, 31-46.

Terzaghi, K., 1943. Theoretical Soil Mechanics. John Wiley and Sons, New York.

Ulusay, R., Aydan, Ö., and Kılıç, R., 2007. Geotechnical assessment of the 2005 Kuzulu landslide (Turkey). Engineering Geology, 89 (1-2), 112-128.